Peer-Reviewed Technical Communication

Adaptive Channel Estimation and Data Detection for Underwater Acoustic MIMO–OFDM Systems

Patricia Ceballos Carrascosa and Milica Stojanovic, *Fellow, IEEE*

***Abstract*—In this paper, frequency and time correlation of the underwater channel are exploited to obtain a low-complexity adaptive channel estimation algorithm for multiple-input–multiple-output (MIMO) spatial multiplexing of independent data streams. The algorithm is coupled with nonuniform Doppler prediction and tracking, which enable decision-directed operation and reduces the overhead. Performance is demonstrated on experimental data recorded in several shallow-water channels over distances on the order of 1 km. Nearly error-free performance is observed for two and four transmitters with BCH(64,10) encoded quadrature phase-shift keying (QPSK) signals. With a 24-kHz bandwidth, overall data rates of up to 23 kb/s after coding were achieved with 2048 carriers. Good results have also been observed in two other experiments with varying MIMO–OFDM (orthogonal frequency-division multiplexing) configurations.**

***Index Terms*—Adaptive channel estimation, multiple-input–multiple-output (MIMO), nonuniform Doppler distortion, orthogonal frequency-division multiplexing (OFDM), underwater acoustic communications.**

I. Introduction

ORTHOGONAL FREQUENCY-DIVISION MULTIPLEXING (OFDM) has recently been investigated for underwater communications as an alternative to single-carrier broadband modulation to achieve high data rate transmission [1]–[5]. It has proved to be an effective technique for combating the multipath delay spread without the need for complex time-domain equalizers.

Multiple transmit and receive antennas can be used to form multiple-input–multiple-output (MIMO) channels to increase the system capacity. The combination of MIMO and OFDM is an appealing low-complexity solution for spectrally efficient communications over bandwidth-limited frequency-selective underwater channels. Previous work on MIMO underwater communications includes spatial multiplexing to increase the bit rate (experimental results have been presented in [4] and [5]), as well as space-time coding to increase link reliability (an Alamouti design has been conceptually described and tested through simulation in [6]). The focus of our present work is on spatial multiplexing of independent data streams.

The most challenging task in a MIMO communication system is channel estimation. Because each received signal contains independent data from all the transmitters, multiple channels have to be estimated simultaneously. Research on wireless radio OFDM systems includes methods that compute the channel impulse response (L coefficients in the time domain) instead of the transfer function (K coefficients in the frequency domain) [7]. A similar method has been pursued for acoustic channels [5]. By doing so, the number of channel parameters is reduced when $L < K$, which is often the case, but this solution may still require inversion of large matrices, whose size is proportional to N_tL, where N_t is the number of transmit elements. In [4], the problem of simultaneous estimation of multiple channels is decomposed into sequential estimation of individual channels by sending pilot tones from one transmitter at a time. In other words, while one transmitter is active, all the other transmitters remain silent. The efficiency of this scheme remains limited to systems with a small number of transmitters (e.g., two). As the number of transmitters grows, so does the overhead (N_tL carriers per transmitter), thus eventually destroying the original goal of using spatial multiplexing to increase the system capacity. Complexity can also be reduced by designing optimal training signals and taking advantage of the channel correlation; namely, by assuming that the channel stays fixed between two adjacent carriers [8], or between two adjacent OFDM blocks [9].

In this work, we focus on the latter type of approaches because of their simplicity. However, we note that these approaches are suboptimal, and that both frequency and time correlation can be better exploited by representing the channel in the impulse response domain, and further modeling the time variation of the so-obtained coefficients. To do so, a series expansion of the time-domain coefficients can be employed, using a chosen set of basis functions, such as complex exponential [10], polynomial [11], or discrete prolate spheroidal [12] functions. Here, we focus on slowly varying channels in which intercarrier interference can be neglected, and restrict our attention to nonmodel-based adaptive channel tracking, using exponential weighting of the past least square (LS) estimates, which offers a suboptimal, but low-complexity alternative to recursive least square (RLS) estimation [13].

Manuscript received June 04, 2008; revised November 18, 2009 and May 20, 2010; accepted May 21, 2010. Date of publication July 29, 2010; date of current version September 01, 2010. This work was supported in part by the Office of Naval Research (ONR) under Grant N00014-07-1-0202 and the ONR Multidisciplinary University Research Initiative (MURI) under Grant N00014-07-1-0738.

Associate Editor: U. Mitra.

P. Ceballos Carracosa is with Telecom UPC, Barcelona 08014, Spain (e-mail: patriciace@gmail.com).

M. Stojanovic is with the Northeastern University, Boston, MA 02115 USA (e-mail: millitsa@ece.neu.edu).

Digital Object Identifier 10.1109/JOE.2010.2052326

To reduce the overhead, we focus on channel estimation that does not require inactive carriers, and makes use of symbol decisions to reduce the number of pilots. Furthermore, we include sparsing of the channel impulse response which was shown to offer improved performance in single-input–multiple-output (SIMO) detection of underwater acoustic OFDM signals [3]. In keeping with the spirit of low-complexity processing, sparsing is based on magnitude truncation, although more advanced methods, such as matching pursuits [14], may hold a promise of improved performance.

The aim of this paper is to demonstrate spatial multiplexing using low-complexity adaptive MIMO processing of experimental OFDM data. The major difference between the wireless radio and acoustic OFDM systems is that the latter suffer from nonuniform frequency offset caused by the motion-induced Doppler effect. Nonuniform Doppler distortion in ultrawideband systems was addressed in [15], where a maximum-likelihood (ML) estimator was provided for the Doppler rate, assuming that it is constant over one OFDM block. The ML solution is computationally intensive, but its performance is close to the Cramer–Rao bound. The need for nonuniform Doppler shift compensation in acoustic OFDM systems was recognized in [16]. A phase prediction method, which is based on adaptive estimation of the Doppler factor, was proposed in [1], and experimentally validated in a SIMO system configuration. Here, we utilize the same principle, extended to a MIMO system configuration. The effectiveness of the algorithm is demonstrated through experimental data processing.

The rest of this paper is organized as follows. In Section II, we introduce the notation and the receiver algorithm. Experimental data results are presented in Section III. Finally, in Section IV, conclusions are summarized.

II. Receiver Algorithm

A. System and Channel Model

We consider a system with N_t transmit and N_r receive elements. Each transmitter is sending an OFDM signal in K subbands, where the input data stream at transmitter t is serial-to-parallel converted into K streams $d_k^t(n),\ k=0,\ldots,K-1$. The block duration is T, and one OFDM block occupies an interval $T' = T + T_g$, where T_g is the guard time which is assumed to contain the multipath spread. The total system bandwidth is B, and the carrier spacing is $\Delta f = 1/T = B/K$. The data symbols $d_k^t(n)$ are assumed to take values from an arbitrary phase-shift keying (PSK) constellation. The symbol rate is $R = K/(T+T_g)$ symbols per second, per transmitter.

Following the approach of [1], the received signal after fast Fourier transform (FFT) demodulation is modeled as

$$y_k^r(n) = \sum_{t=1}^{N_t} H_k^{\mathrm{tr}}(n) d_k^t(n) e^{j\theta_k^t(n)} + z_k^r(n) \tag{1}$$

where the indices t, r, k, n refer to the transmitter, receiver, subband, and time, respectively. The coefficient $H_k^{\mathrm{tr}}(n)$ represents the transfer function of the channel between transmitter t and receiver r, evaluated at frequency $f_k = f_0 + k\Delta f$ during the nth OFDM block. The phase $\theta_k^t(n)$ represents the offset caused by the motion-induced Doppler effect, which is assumed to be equal for all receivers, but may differ between the transmitters. Specifically, the phase distortion is modeled as

$$\theta_k^t(n) = \theta_k^t(n-1) + a^t(n) 2\pi f_k T' \tag{2}$$

where $a^t(n)$ is the residual Doppler factor after initial signal resampling. It is assumed to be constant during one OFDM block, but may change from one block to another. Specifically, if $a'^t(n) = v^t(n)/c$ denotes the ratio of relative transmitter–receiver velocity to the speed of sound, i.e., the Doppler rate of the received signal, and initial resampling is performed over several blocks using an estimate a'', then the residual Doppler factor is $a^t(n) = (a'^t(n) - a'')/(1 + a'^t(n))$ [17]. Model (1)–(2) holds so long as the Doppler shift is much less than the carrier spacing, i.e., $a^t(n) f_k \ll \Delta f,\ \forall k, n, t$. The residual intercarrier interference is then treated as additional noise, contained in the term $z_k^r(n)$.

Let us now form the vectors

$$\mathbf{y}_k(n) = [y_k^1(n), \ldots, y_k^{N_r}(n)]^T \tag{3}$$
$$\mathbf{d}_k(n) = [d_k^1(n), \ldots, d_k^{N_t}(n)]^T \tag{4}$$
$$\mathbf{z}_k(n) = [z_k^1(n), \ldots, z_k^{N_r}(n)]^T \tag{5}$$

and the matrices

$$\mathbf{H}_k(n) = \begin{bmatrix} H_k^{11}(n) & \cdots & H_k^{N_t 1}(n) \\ \vdots & & \vdots \\ H_k^{1 N_r}(n) & \cdots & H_k^{N_t N_r}(n) \end{bmatrix} \tag{6}$$
$$\mathbf{\Theta}_k(n) = \mathrm{diag}\left[e^{j\theta_k^1(n)}, \ldots, e^{j\theta_k^{N_t}(n)}\right]. \tag{7}$$

Using this notation, we have that

$$\mathbf{y}_k(n) = \mathbf{H}_k(n)\mathbf{\Theta}_k(n)\mathbf{d}_k(n) + \mathbf{z}_k(n). \tag{8}$$

B. Data Detection

Given the channel matrix and the phases, the LS estimate of the data symbols transmitted on the kth carrier follows from the expression (8), and it is given by

$$\hat{\mathbf{d}}_k(n) = \mathbf{\Theta}_k^{-1}(n)[\mathbf{H}_k'(n)\mathbf{H}_k(n)]^{-1}\mathbf{H}_k'(n)\mathbf{y}_k(n) \tag{9}$$

where the prime denotes conjugate transpose. Since the channel and the phase are not known in practice, their estimates will be used instead of the true values. Data detection is performed by soft (or hard) decision decoding of the estimates (9).

C. Channel Estimation

In each OFDM block, $N_t N_r$ channel coefficients have to be estimated for each subband. However, only N_r observations of the received signal $y_k^r(n)$ are available for each k. To increase the number of observations, we will exploit both the frequency and the time correlation of the channel.

1) Frequency Correlation: Assuming that the channel transfer function for each transmitter–receiver pair is the same over M_f adjacent carriers,[1] we have that

$$H_{k+i}^{\mathrm{tr}}(n) = H_k^{\mathrm{tr}}(n), \qquad i = 1, \ldots, M_f - 1. \tag{10}$$

Using this assumption, and defining the following quantities:

$$\check{\mathbf{y}}_k^r(n) = \left[y_k^r(n), \cdots, y_{k+M_f-1}^r(n)\right]^T \tag{11}$$

$$\check{\mathbf{z}}_k^r(n) = \left[z_k^r(n), \ldots, z_{k+M_f-1}^r(n)\right]^T \tag{12}$$

$$\mathbf{H}_k^r(n) = \left[H_k^{1r}(n), \ldots, H_k^{N_t r}(n)\right]^T \tag{13}$$

$$\check{\mathbf{d}}_k(n) = \left[d_k^1(n)e^{j\theta_k^1(n)}, \ldots, d_k^{N_t}(n)e^{j\theta_k^{N_t}(n)}\right] \tag{14}$$

$$\check{\mathbf{D}}_k(n) = \begin{bmatrix} \check{\mathbf{d}}_k(n) \\ \vdots \\ \check{\mathbf{d}}_{k+M_f-1}(n) \end{bmatrix} \tag{15}$$

we can write

$$\check{\mathbf{y}}_k^r(n) = \check{\mathbf{D}}_k(n)\mathbf{H}_k^r(n) + \check{\mathbf{z}}_k^r(n). \tag{16}$$

This model serves as a basis for channel estimation. A necessary condition for the matrix $\check{\mathbf{D}}_k(n)$ to have full column rank is that $M_f \geq N_t$. Note that the channel is estimated individually for every receiving element; hence, spatial correlation (if any) is not exploited at this point. Multichannel combining is performed later to yield the data estimates (9). Depending on the range of subbands k for which assumption (10) is made and model (16) formed, we distinguish between two types of channel estimates: one based on a fixed window, and another based on a sliding window of subbands.

In the case of *fixed window estimation*, the received signal observations are divided into K/M_f groups of M_f subbands,[2] where $M_f \geq N_t$. Each group of subbands is now treated independently, and a single estimate is obtained for all the subbands in that group. In other words, assumption (10) is made for $k = 0, M_f, \ldots (K/M_f - 1)M_f$, and model (16) is applied for the same range of k.

Given the data symbols and the phases, the LS estimate of the channel at each receiving element is given by

$$\hat{\mathbf{H}}_k^r(n) = [\check{\mathbf{D}}_k'(n)\check{\mathbf{D}}_k(n)]^{-1}\check{\mathbf{D}}_k'(n)\check{\mathbf{y}}_k^r(n) \tag{17}$$

where $k = 0, M_f, \ldots (K/M_f - 1)M_f$. The remaining estimates are obtained using assumption (10), i.e., $\hat{\mathbf{H}}_{k+i}^r(n) = \hat{\mathbf{H}}_k^r(n)$ for $i = 1, \ldots, M_f - 1$.

Since the data and the phases are not known, the symbol decisions and phase estimates will be used instead. Assuming that the channel does not change much during adjacent OFDM blocks, the channel estimates from a previous block are used to make tentative symbol decisions that will in turn be used to update the phase and the current channel estimate. Note that pilot tones can also be used to aid decision-directed operation, but their number does not need to be constrained by the channel length as in [4].

In the case of *sliding window estimation*, the first group of observations is defined as before, $y_0^r(n), y_1^r(n), \ldots y_{M_f-1}^r(n)$, and the initial channel estimate is obtained from it. Starting from here, each new group is defined by sliding the window of size M_f by one, to compute the channel estimate at the next carrier. Modeling equation (16) remains the same, but the estimates are computed for all $k = 0, 1, \ldots K - M_f$. Specifically, we associate a channel estimate obtained from a group of observations with the midfrequency occupied by that group

$$\hat{\mathbf{H}}_{k+M_f/2-1}^r(n) = [\check{\mathbf{D}}_k'(n)\check{\mathbf{D}}_k(n)]^{-1}\check{\mathbf{D}}_k'(n)\check{\mathbf{y}}_k^r(n) \tag{18}$$

where $k = 0, 1, \ldots K - M_f$. The band-edge estimates are set to

$$\hat{\mathbf{H}}_i^r(n) = \hat{\mathbf{H}}_{M_f/2-1}^r(n), \qquad \text{for } i = 0, \ldots M_f/2 - 2$$
$$\hat{\mathbf{H}}_i^r(n) = \hat{\mathbf{H}}_{K-M_f/2-1}^r(n), \qquad \text{for } i = K - M_f/2, \ldots K - 1.$$

The sliding window method requires more computations, but gives a better performance than the fixed window method.

Fig. 1 illustrates the operation of the two methods for an example with $M_f = 4$. For simplicity, a single receiving element is assumed. In the case of fixed window estimation, the first four observations $y_0(n), y_1(n), y_2(n), y_3(n)$ are used to form $\hat{H}_0(n)$. This estimate is used for all four subbands, i.e., $\hat{H}_0(n) = \hat{H}_1(n) = \hat{H}_2(n) = \hat{H}_3(n)$. The same principle is applied to the next four observations $y_4(n), y_5(n), y_6(n), y_7(n)$, and so on. In the case of sliding window estimation, the observations from the first four subbands are used to form $\hat{H}_1(n)$, which is extrapolated to all lower subbands, $\hat{H}_0(n) = \hat{H}_1(n)$ in this case. The next estimate $\hat{H}_2(n)$ is obtained by sliding the window to capture $y_1(n), y_2(n), y_3(n), y_4(n)$, and so on. The last estimate will be extrapolated to the remaining subbands at the high band edge.

Note also that a sliding window approach can effectively be implemented in a recursive manner, so that the full solution (18) does not need to be computed for every carrier. The initial channel estimate can be formed using the signals on the first M_f carriers as before, and a recursive update can follow. For example, a least mean square (LMS) recursion is given by

$$\hat{\mathbf{H}}_{k+m}^r(n) = \hat{\mathbf{H}}_{k+m-1}^r(n) + \mu\check{\mathbf{D}}_k(n)[\check{\mathbf{y}}_k^r(n) - \check{\mathbf{D}}_k(n)\hat{\mathbf{H}}_k^r(n)]'$$

where $m = M_f/2 - 1$ and μ is the step size. The LMS algorithm eliminates the need for matrix inversion, thus reducing the computational complexity. However, note that complexity is not overwhelming for small values of M_f, e.g., 2–4, and we will accordingly use the full solution (18) when discussing the experimental results.

To carry out the channel estimation as described so far, the channel transfer function has to be assumed constant over $M_f \geq N_t$ adjacent carriers to provide a sufficient number of observations. Since the coherence frequency of the channel is given by the inverse of its multipath spread T_{mp}, M_f has to be chosen such that

$$M_f \Delta f \ll 1/T_{mp}. \tag{19}$$

[1] This approach is taken in [8] for two carriers.

[2] Without the loss of generality, we assume that M_f is even, and that K/M_f is an integer.

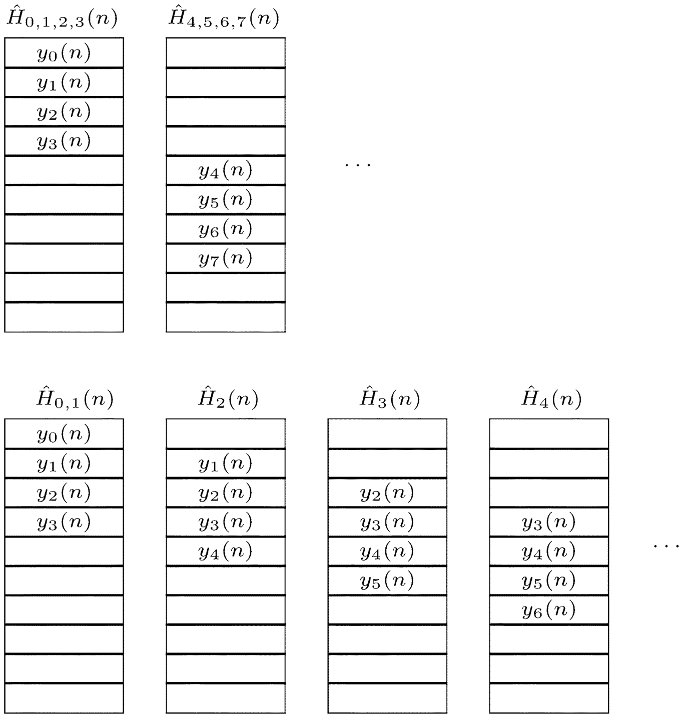

Fig. 1. Channel estimation using fixed window (top) or sliding window (bottom) with $M_f = 4$. In the fixed window case, the signals $y_k(n)$ observed on four adjacent carriers are used to form an estimate of the channel transfer function, which is then associated with all four corresponding carriers. In the sliding window case, the channel estimate is associated with a middle carrier, and the window is moved by one to continue the process.

This assumption is more easily justified when a greater number of carriers K is used in a given bandwidth B, as the subband width $\Delta f = B/K$ is then narrower. A greater number of subbands also implies a greater bandwidth efficiency, defined (for each transmitter) as the ratio of the symbol rate R to the occupied bandwidth B

$$\frac{R}{B} = \frac{K/(T+T_g)}{K/T} = \frac{1}{1+\alpha} \tag{20}$$

where $\alpha = T_g(B/K)$. Hence, it is advantageous to use large K, both from the viewpoint of maximizing the bandwidth efficiency, and from the viewpoint of satisfying assumption (10).

The greatest number of subbands that can be used in a given system is limited by two factors: 1) the motion-induced Doppler shift, and 2) the temporal coherence of the channel (the Doppler spread corresponding to the inherent channel variation, regardless of the motion). Specifically, we recall that post-FFT processing is based on the assumption of small residual Doppler shift, i.e., $a^t(n) f_k \ll \Delta f$, $\forall t, k, n$. In order for this assumption to hold, the number of subbands has to be

$$K \ll \frac{1}{a^t(n)(1+f_0/B)} \qquad \forall t, n. \tag{21}$$

If this condition is not satisfied, the signals will shift out of their allocated subbands, causing both a loss of phase coherence in the desired signal and intercarrier interference. Basic model (1) will then no longer hold, and the simple post-FFT processing, which is based on it, will fail.

The second factor, namely the temporal channel coherence, refers to the fact that even in the absence of motion-induced Doppler distortion $(a^t(n) = 0)$, the channel coefficients $H_k^{\mathrm{tr}}(n)$ may be varying in time. Adaptive decision-directed receiver operation is based on the assumption that this variation is slow, so that the channel does not change much from one block to another. The validity of such an assumption depends on the relationship between the interblock separation T' and the coherence time of the channel, which is proportional to the inverse of its inherent Doppler spread B_d. Clearly, in order for $T' \ll 1/B_d$ to hold, the block duration T must be limited, i.e., for a fixed bandwidth B, the number of carriers $K = BT$ cannot exceed this coherence limit.

Ideally, K will be large enough so that good bandwidth efficiency is achieved, while the corresponding Δf is small enough for assumption (19) to hold. If this is not the case, it will not be possible to exploit the frequency correlation (10) to obtain a sufficient number of observations for channel estimation. In such a case, one may resort to exploiting the time correlation between adjacent OFDM blocks.

2) Time Correlation: Time correlation is exploited by assuming that the channel transfer function does not change between M_t consecutive OFDM blocks,[3] i.e.,

$$H_k^{\mathrm{tr}}(n) = H_k^{\mathrm{tr}}(n-m), \qquad m = 1, \ldots, M_t - 1. \tag{22}$$

The channel estimation problem can now be redefined to include this assumption in addition to the frequency correlation assumption (10). In particular, we define the vector of $M = M_t M_f$ observations as

$$\check{\mathbf{y}}_k^r(n) = \begin{bmatrix} y_k^r(n-M_t+1) \\ \vdots \\ y_k^r(n) \\ \hdashline \vdots \\ \hdashline y_{k+M_f-1}^r(n-M_t+1) \\ \vdots \\ y_{k+M_f-1}^r(n) \end{bmatrix} \tag{23}$$

and the corresponding data matrix as

$$\check{\mathbf{D}}_k(n) = \begin{bmatrix} \check{\mathbf{d}}_k(n-M_t+1) \\ \vdots \\ \check{\mathbf{d}}_k(n) \\ \hdashline \vdots \\ \hdashline \check{\mathbf{d}}_{k+M_f-1}(n-M_t+1) \\ \vdots \\ \check{\mathbf{d}}_{k+M_f-1}(n) \end{bmatrix}. \tag{24}$$

We now have the modeling equation in the same form (16) as before, but with the newly defined observation vector and the data matrix. The number of observations needed for each

[3]This approach is taken in [9] for two blocks.

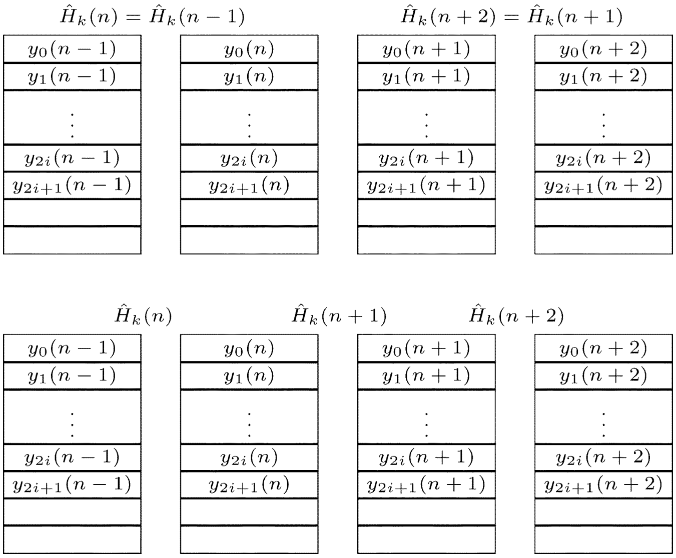

Fig. 2. Channel estimation using fixed window in time (top) and sliding window (bottom) with $M_t = 2$, and a fixed window of size $M_f = 2$ in frequency. In the fixed window case, two adjacent blocks in time are used to form a channel estimate (for each carrier), which is then associated with both corresponding blocks. In the sliding window case, the estimate is associated with one of the blocks (in general, a middle block), and the window is moved by one to continue the process.

estimate now has to be $M_t M_f \geq N_t$. As before, fixed window (17) or sliding window estimation (18) can be performed. The concept of a "window" now extends into the time domain, as illustrated in Fig. 2. For simplicity, this figure refers to a single receiving element and a fixed window in frequency. $M = 4$ observations are collected assuming that the channel stays the same over $M_f = 2$ adjacent subbands and $M_t = 2$ adjacent OFDM blocks.

Starting with the blocks $n-1$ and n, the next time window can be constructed in a fixed fashion (blocks $n+1$ and $n+2$) or in a sliding fashion (blocks n and $n+1$). In decision-directed mode, the currently available estimates $\hat{H}_k^{\text{tr}}(n)$ must be used to obtain tentative symbol decisions for the next block(s). The sliding time window requires only one new block worth of data symbols, and may be preferable over the fixed window on a time-varying channel. In this approach, tentative decisions for the $(n+1)$th block are used together with the already existing past decisions to form the data matrix $\check{\mathbf{D}}_k(n+1)$, which is then used to calculate the estimates $\hat{\mathbf{H}}_k^r(n+1)$.

To exploit the time correlation of the channel by combining adjacent blocks, M_t has to be chosen such that

$$M_t T' \ll 1/B_d \tag{25}$$

where $T' = T(1+\alpha)$, and α is the factor associated with the bandwidth efficiency (20). Combining this condition with the frequency coherence requirement (19), we find that the total number of observations $M = M_t M_r$ has to satisfy

$$N_t \leq M \ll \frac{1}{B_d T_{mp}} \frac{1}{1+\alpha}. \tag{26}$$

This condition implies that regardless of M, there is a limit on the total number of transmit elements that can be used with low-complexity processing, and this limit depends on the coherence properties of the channel. However, so long as the channel is underspread, i.e., $B_d T_{mp} \ll 1$, the coherence condition will be satisfied for a reasonable number of transmit elements. For example, if $B_d = 1$ Hz and $T_{mp} = 10$ ms, and the bandwidth efficiency per transmitter is only $1/2(\alpha = 1)$, we have that $N_t \ll 50$. Nonetheless, it must be kept in mind that acoustic channels with much worse coherence properties and delay spreads have been observed (e.g., $T_{mp} = 100$ ms and $B_d = 10$ Hz), and that condition (26) has to be checked before designing and deploying the system.

As far as the receiver design is concerned, there are several tradeoffs in choosing the value of M, and, more specifically, the values of M_f and M_t. In general, M can be as low as N_t. This choice has the advantage of lowest computational complexity, as well as the least restrictive coherence requirements. However, it suffers most from the estimation noise, and is also associated with the highest incidence of singular data matrices (we will comment more on this issue when we discuss the experimental results). Consequently, it may be advantageous to use M somewhat greater than the minimum, e.g., $M = 2N_t$ (this choice provided uniformly good results with experimental signals).

Once the value of M has been fixed, M_f and M_t should be determined in accordance with the frequency and time coherence requirements (19) and (25). These requirements must be weighed in light of the number of carriers K used in a given bandwidth. Specifically, they imply the following constraint:

$$M_f B T_{mp} \ll K \ll \frac{B}{M_t B_d (1+\alpha)}. \tag{27}$$

Recalling that bandwidth efficiency improves with K, we note that the preferred system design is one with M_t as low as possible, e.g., $M_t = 1$. Solutions with $M_t > 1$ should be sought only when frequency coherence cannot be guaranteed over sufficiently many subbands (at least N_t are needed for channel estimation), and carrier separation cannot be further reduced, e.g., because of the synchronization requirement (21). Roughly speaking, for a small carrier separation Δf, more emphasis will be placed on exploiting the frequency correlation $(M_f > M_t)$, while for a large carrier separation, the emphasis will shift to exploiting the time correlation $(M_t > M_f)$. Note also that the interpretation of the "much less" sign is a soft one, and that system design ultimately has to be judged in a field test. We will comment more on these tradeoffs when we discuss the particular examples in Section III.

D. Adaptive Channel Tracking

Channel estimates (17) can additionally be smoothed by adaptive filtering. This can be performed directly on the transfer function coefficients to obtain

$$\hat{\mathbf{H}}_k^r(n) = \lambda \hat{\mathbf{H}}_k^r(n-1) + (1-\lambda)\mathbf{X}_k^r(n) \tag{28}$$

where $\lambda \in [0,1)$ accounts for the filter memory, and we have used $\mathbf{X}_k^r(n)$ to rename the one-shot estimate (17)

$$\hat{\mathbf{X}}_k^r(n) = [\check{\mathbf{D}}_k'(n)\check{\mathbf{D}}_k(n)]^{-1}\check{\mathbf{D}}_k'(n)\check{\mathbf{y}}_k^r(n). \tag{29}$$

TABLE I
EXPERIMENT SETTINGS

Experiment	N_t	N_r	Distance [m]	Frequency Band [kHz]	K	T [ms]	T_g [ms]	$R/B = \frac{T}{T+T_g}$
1 : FL	2, 4	8	500, 1000, 1500	24 − 48	128 − 2048	5.3 − 85.3	25	0.175 − 0.773
2 : MA	2	6	600	75 − 137.5	1024 − 4096	16.4 − 65.5	16	0.506 − 0.804
3 : RI	2	6	400, 1000	10 − 12.4	128 − 256	52.4 − 104	15	0.777 − 0.874

Alternatively, the update can be performed on the impulse response coefficients, which are defined through the discrete Fourier transform (DFT) pair

$$H_k^{tr}(n) = \sum_{l=0}^{K-1} h_l^{tr}(n)e^{-j2\pi k(l/K)} \qquad \forall t, r. \tag{30}$$

Taking the DFT of both sides of expression (28), we have that

$$\hat{\mathbf{h}}_l^r(n) = \lambda\hat{\mathbf{h}}_l^r(n-1) + (1-\lambda)\mathbf{x}_l^r(n) \tag{31}$$

where

$$\hat{\mathbf{h}}_l^r(n) = \left[\hat{h}_l^{1r}(n), \ldots, \hat{h}_l^{N_t r}(n)\right]^T \tag{32}$$

and $\mathbf{x}_l^r(n)$ is the inverse DFT

$$\mathbf{x}_l^r(n) = \frac{1}{K}\sum_{k=0}^{K-1} \mathbf{X}_k^r(n)e^{j2\pi k(l/K)}. \tag{33}$$

Hence, N_t FFTs of size K are needed to arrive at the update (31). However, this approach has an advantage in that it allows channel sparsing.

E. Channel Sparsing

While all K channel coefficients $\hat{H}_k^{tr}(n)$ are required per transmitter–receiver pair, fewer than K coefficients $\hat{h}_l^{tr}(n)$ may be needed to completely describe the channel. For a wideband signal, the significant coefficients in the impulse response domain correspond to the physical propagation paths. By eliminating those coefficients $\hat{h}_l^{tr}(n)$ whose amplitude falls below a certain threshold (e.g., 15 dB below the maximum), the total estimation noise is reduced, and the performance can be improved [3].

Specifically, let us say that there are J significant coefficients in the impulse response domain $\hat{h}_{l_j}^{tr}(n)$, $j = 1, \ldots, J$. These coefficients are identified from the estimates $\hat{h}_l^{tr}(n)$ and used to form the truncated estimates

$$\tilde{h}_l^{tr}(n) = \begin{cases} \hat{h}_l^{tr}(n), & \text{if } |\hat{h}_l^{tr}(n)| \geq \gamma \max_l \left\{\left|\hat{h}_l^{tr}(n)\right|\right\} \\ 0, & \text{otherwise} \end{cases} \tag{34}$$

where $\gamma \in [0, 1)$ represents the truncation threshold.

The truncated, or sparse, estimates $\tilde{h}_l^{tr}(n)$ are now used to recalculate the transfer function coefficients

$$\tilde{H}_k^{tr}(n) = \sum_{l=0}^{K-1} \tilde{h}_l^{tr}(n)e^{-j2\pi k(l/K)}, \qquad k = 0, \ldots, K-1. \tag{35}$$

These coefficients are finally used to perform data detection.

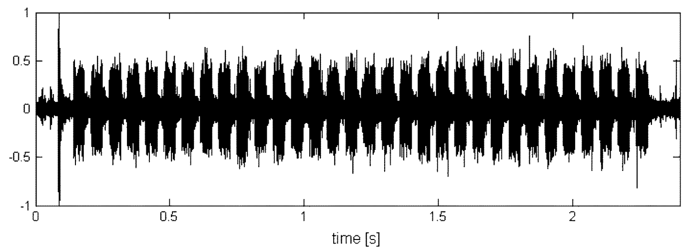

Fig. 3. Received signal in Experiment 1, for a $K = 1024$ frame with four transmitters at a transmission distance of 1500 m. Shown are the preamble and $N_d/K = 32$ OFDM blocks.

If the positions of significant impulse response coefficients do not change from one block to another, the update (31) can be performed only for those coefficients. However, if there is drifting of the coefficients, or if new ones appear and the old ones disappear, then the update (31) should be performed for all l.

A complete summary of the algorithm is given in the Appendix. The complexity of the algorithm is dominated by matrix inversions, of which there are at most K per OFDM block, each of size $N_t \times N_t$. Because N_t is usually a small number, and because these operations can be carried out in parallel for different carriers, the overall complexity remains low compared to the methods such as [7], which require inversion of a single matrix for all carriers, but its size is $N_tL \times N_tL$, where L is proportional to the total multipath spread of the channel $L \sim BT_{mp}$.

III. Experimental Results

The focal point of our work is experimental analysis of MIMO–OFDM over bandlimited acoustic channels, where an increase in bit rate is sought through spatial multiplexing of independent data streams. The receiver algorithm has been tested in three different MIMO–OFDM experiments. Table I summarizes the salient features of the signals used in these experiments. In each experiment, one transmitter has been activated at a time, and the received signals were later combined to mimic a varying number of transmitters. All the data were collected by the Woods Hole Oceanographic Institution (WHOI, Woods Hole, MA).

A. Experiment 1: Panama City Beach, FL

Experiment 1 was part of the "AUV Fest," held at the Panama City Beach, FL, in June 2007. The transmitter and the receiver were deployed about 9 m below the surface in 20-m-deep water. The signals were sent from four equally spaced elements, with a total vertical aperture of 1 m. The vertical receiving array was 2 m in aperture with eight elements equally spaced at 25 cm.

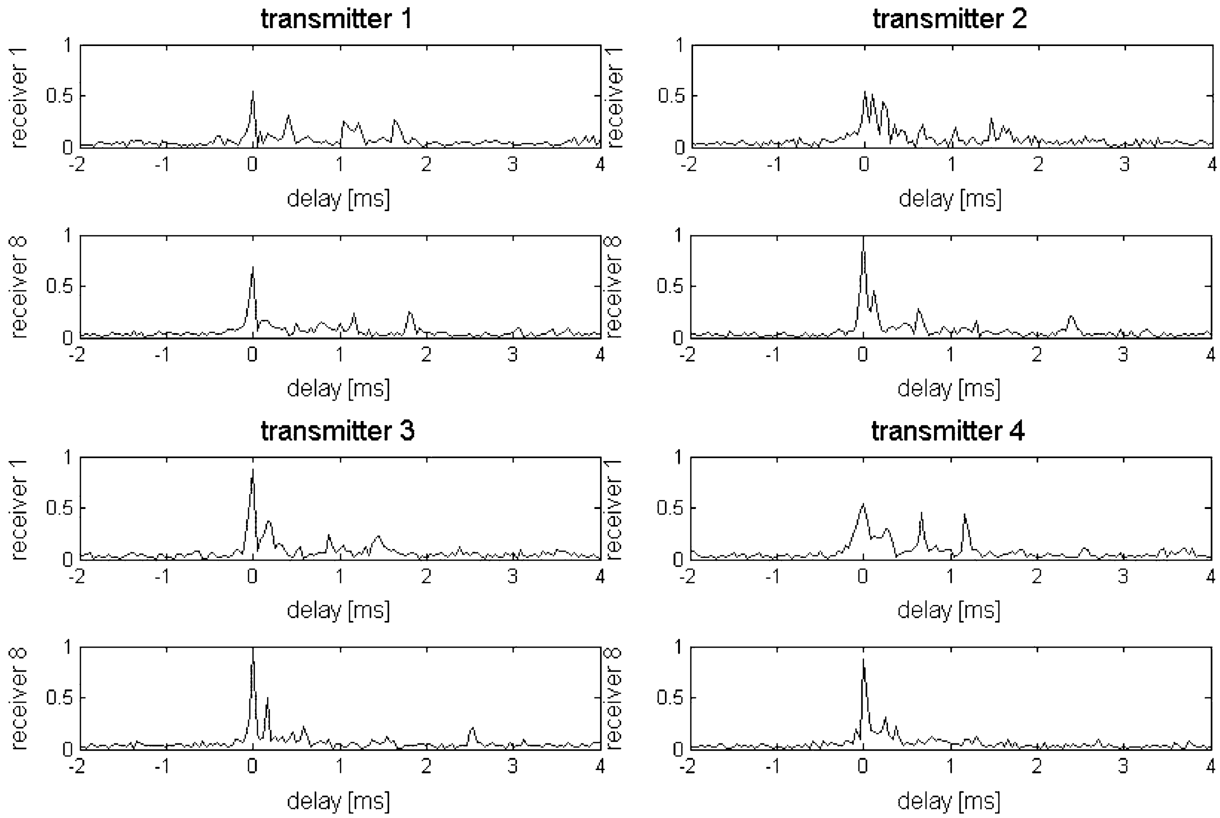

Fig. 4. Channel estimates in Experiment 1 (magnitude of the impulse response) for a frame with $K = 1024$ carriers and four transmitters at a distance of 1500 m.

The center frequency was 36 kHz, with a 24-kHz bandwidth. The sampling rate was 96 kHz.

In this experiment, $N_d = 32\,768$ quadrature phase-shift keying (QPSK) symbols per transmitter were sent from either two or four transmitters (chosen as maximally spaced), using a varying number of subbands ranging from 128 to 2048. The guard interval was chosen to be $T_g = 25$ ms with zero padding. The signals were coded using the BCH(64,10) code. This code was selected so as to match the one currently implemented in the WHOI modem. Each string of 10 b was encoded into a 32-symbol QPSK codeword, until K symbols were obtained. These symbols were then assigned to the OFDM carriers in such a manner that the symbols of one codeword were maximally separated in frequency. Soft decision decoding was employed. Confining the codewords to the same OFDM block does not exploit time diversity, but it enables instantaneous decoding, thus providing reliable tentative decisions in the loop of adaptive channel/phase estimator.

Fig. 3 shows the received signal from a frame with four transmitters and 1024 carriers. The frame preamble is a pseudonoise (PN) sequence of length 127, quadrature modulated at 24 kilosymbols per second (ksps) using the center frequency of 36 kHz. Frame synchronization is performed by matched filtering to the preamble.

Channel estimates for this frame are shown in Fig. 4. Channel estimation is performed for all transmitter–receiver pairs using the sliding window technique in both frequency and time. Shown are the results for all transmitting elements, the top and the bottom receiving element. From the 1024 coefficients that are computed for each transmitter–receiver pair, only between 9 and 30 are preserved after channel sparsing (threshold $\gamma = 0.2$). The different peaks in the channel estimates can be associated with multiple surface and bottom reflections calculated from the geometry of the experiment.

The phase estimates are shown in Fig. 5. The estimated Doppler factors $\hat{a}^t(n)$ range between -5×10^{-5} and 5×10^{-5}. It is interesting to note that although the transmit elements are close together, their phases may differ significantly. This behavior can be explained by noting that tilting of the common transmitter frame structure can cause each transmitter's relative motion to be different with respect to the receiver array. Individual phase estimation for each transmitter proved to be crucial for successful data detection in this experiment.

Table II provides the summary of algorithm performance with two transmitters. $M = 2N_t = 4$ observations were used, and various combinations of M_f and M_t were investigated for each value of K. Listed in the table are those combinations that provided the best performance. As expected, $M_t \times M_f = M \times 1$ was the best choice for the lowest value of K, shifting to $1 \times M$ for higher values of K and narrower carrier separations Δf. The results provided are for one frame of data sent ($N_d = 32\,768$ QPSK symbols per transmitter) with $N_p = K/32$ pilots. No degradation in performance was observed without the use of pilot tones, except with $K = 2048$. The bit error rate (BER) indicated in the table represents the ratio of erroneously decoded bits to the total number of bits transmitted, averaged over all transmitters. We observe that excellent results are achieved in this experiment. BER on the order of 5×10^{-2} is obtained without

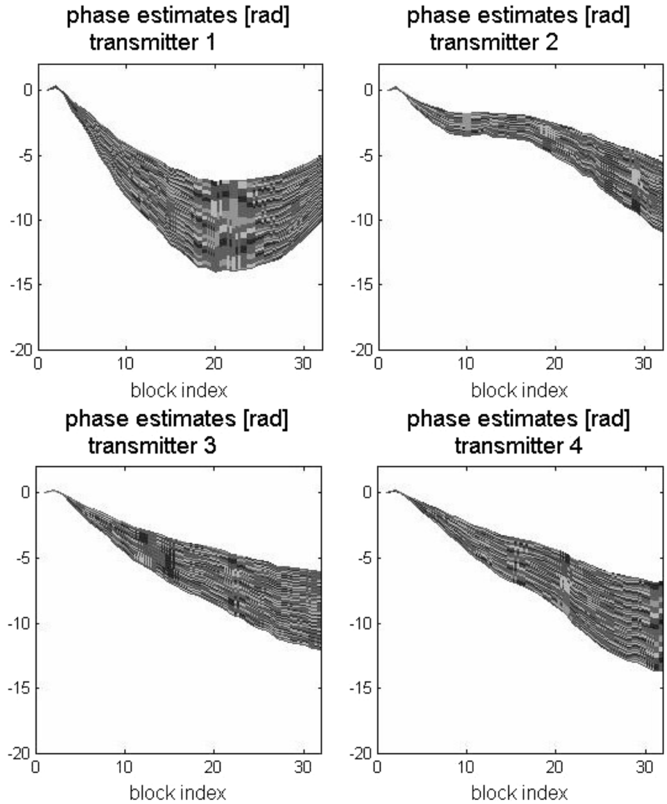

Fig. 5. Phase estimates in Experiment 1 for all carriers (nonuniform compensation) for a frame with $K = 1024$ at a transmission distance of 1500 m.

TABLE II
EXPERIMENT 1: RESULTS FOR SEVERAL MIMO CONFIGURATIONS WITH TWO TRANSMITTERS

$\mathbf{K}$	**128**	**256**	**512**	**1024**	**2048**
$\mathbf{\Delta f}[Hz]$	187.5	93.75	46.88	23.44	11.72
$\mathbf{T}[ms]$	5.3	10.7	21.3	42.7	85.3
$\mathbf{M_t} \times \mathbf{M_f}$	4×1	2×2	1×4	1×4	1×4
BER(500 m)	0	0	0	0	0
BER(1000 m)	0	0	0	0	0
BER(1500 m)	0	0	0	0	0

coding, indicating that a lower rate code could be used in these conditions. We also note that the guard time of 25 ms was unnecessarily long; 5 ms would have sufficed for this channel, yielding a higher bandwidth efficiency.

Performance of the receiver for $K = 1024$ carriers at a transmission distance of 1000 m is detailed in Fig. 6, which shows the scatter plot of the symbol estimates and the corresponding mean squared error over time and carriers. Shown also are the phase estimates, the Doppler factor, and the impulse response estimate before sparsing.

Results for four transmitters are summarized in Table III. $M = 2N_t = 8$ observations were used in this case. As before, the results refer to one frame of data sent ($N_d = 32\,768$ QPSK symbols per transmitter) with $N_p = K/32$ pilots per transmitter. The BER indicated in the table is that after decoding;

TABLE III
EXPERIMENT 1: RESULTS FOR SEVERAL MIMO CONFIGURATIONS WITH FOUR TRANSMITTERS

$\mathbf{K}$	**128**	**256**	**512**	**1024**	**2048**
$\mathbf{\Delta f}[Hz]$	187.5	93.75	46.88	23.44	11.72
$\mathbf{T}[ms]$	5.3	10.7	21.3	42.7	85.3
$\mathbf{M_t} \times \mathbf{M_f}$	8×1	4×2	4×2	2×4	1×8
BER (500 m)	0×1	4×10^{-3}	4×10^{-3}	10^{-3}	4×10^{-3}
BER (1000 m)	0×2	10^{-3}	8×10^{-4}	2×10^{-3}	9×10^{-3}
BER (1500 m)	3×10^{-3}	10^{-3}	0	0	0

without coding, the BER is on the order of 0.15. Compared with the two-transmitter case, the performance is degraded due to the greater amount of crosstalk between the channels, and the increased vulnerability of coherence assumptions at $M = 8$ as opposed to $M = 4$.

We observe that $K = 128$ is a poor design choice in this case, most likely because it challenges the frequency coherence assumption (19). It is also interesting to note that performance tends to improve with transmission distance, which can be explained by an increasing coherence frequency (decreasing multipath spread). For example, if the system geometry is used to compute the delay spread of the surface–bottom–surface reflection (2.2, 1.1, and 0.75 ms), the corresponding coherence frequency is found to be 450, 900, and 1350 Hz for the transmission distance of 500, 1000, and 1500 m, respectively. A similar calculation can be made for the later reflections as well, but the surface–bottom–surface path suffices to illustrate the argument. Hence, the frequency coherence assumption is more easily justified at longer ranges. These numbers also support the fact that performance improves for higher values of K. Notably, for K =512, 1024, and 2048, $M_f \Delta f = 93.75$ Hz, and, at least for 1500 m, frequency coherence can be assumed. It may be worth noting that at this distance, $K = 512$ and 1024 offered equally good performance without pilot assistance.

For both two and four transmitters, at least under the conditions of the present experiment and for the bandwidth used, the best performance of the algorithm was observed with 512 and 1024 carriers. These design choices resulted in consistently good performance, monitored over multiple signal frames. As K further increases, the limit imposed by the phase coherence of channel (21) is occasionally reached, causing a failure with $K = 2048$, particularly at shorter distances.

While the above results were obtained using $M = 2N_t$ observations, good performance was also achieved with $M = N_t$ observations, which further reduces the computational complexity. However, as the size of the matrix $\check{\mathbf{D}}_k(n)$ is reduced, the chances of its leading to an ill-posed channel estimation problem increase. Namely, this matrix depends on the random values of the data symbols in a current block, and, hence, it can happen that its inverse, or pseudoinverse for $M > N_t$, does not exist. In such a

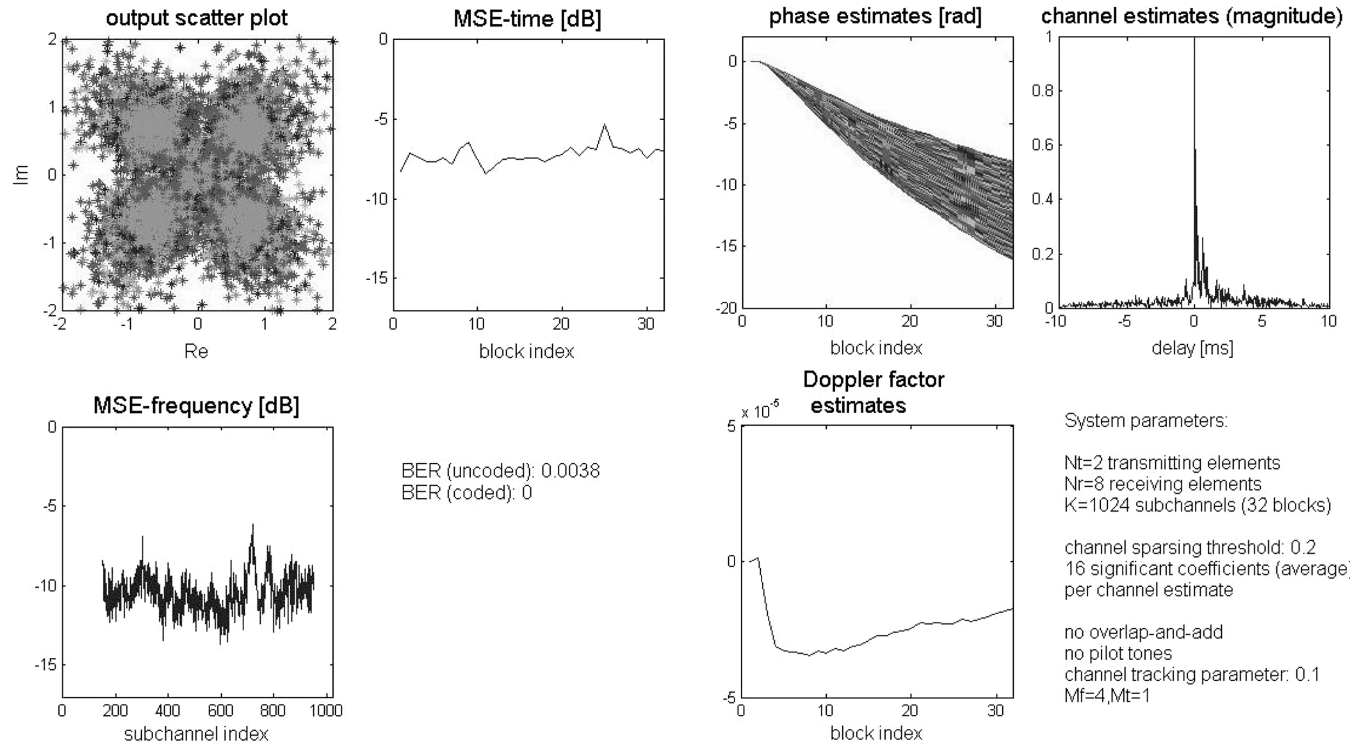

Fig. 6. Signal processing results for Experiment 1 at a transmission distance of 1000 m. Band-edge carriers were disabled to avoid the transducer cutoff.

case, the new channel estimate cannot be computed, and the previous channel estimate is kept instead. This simple method provided excellent results in the present experiment. For example, with $K = 2048$, four transmitters, and a distance of 1500 m, error-free performance was obtained with $M_t \times M_f = 1 \times 4$ (instead of 1×8), although an average of 50 out of the 2048 inversions were skipped due to the matrix singularity (only 12 instances of singularity were observed for $M_t \times M_f = 1 \times 8$).

Sliding window estimation has been used both in time and in frequency. To reduce the complexity, fixed window can be used in frequency without performance degradation, except with $M_t \times M_f = 1 \times 8$. When operating in a decision-directed mode, sliding window in time was found to be necessary.

B. Experiment 2: Buzzards Bay, MA

The data in this experiment were collected in Buzzards Bay, MA, in March 2008. The transmitter and the receiver were deployed about 6 m below the surface in 12-m-deep water and separated by 600 m. The signals were transmitted from two elements separated by 0.6 m. The vertical receiving array was composed of six elements, equally spaced at 0.2 m. In this experiment, a very-high-frequency (VHF) signal was used, occupying the bandwidth between 75 and 137.5 kHz. The sampling rate was 1 MHz.

$N_d = 32\,768$ QPSK symbols per frame were transmitted from each transmitter, using a varying number of subbands ranging from 1024 to 4096. The guard interval was chosen to be $T_g = 16$ ms. The signals were coded using the BCH(64,10) code.

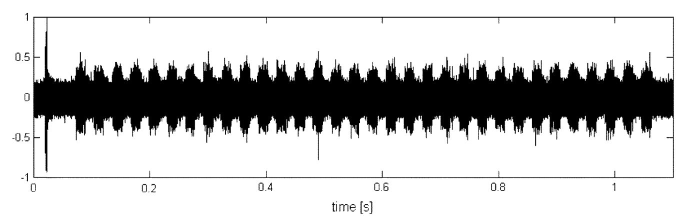

Fig. 7. Received signal in Experiment 2, for a $K = 1024$ frame with two transmitters at a transmission distance of 600 m. Shown are the preamble and $N_d/K = 32$ OFDM blocks.

Fig. 7 shows the received signal from a frame with two transmitters and $K = 1024$ carriers. Compared to the previous experiment, the signal is obviously much more affected by noise, which appears to be the major limitation in this experiment.

Performance of the algorithm is summarized in Table IV. The receiver was configured to operate with $N_p = K/32$ pilots and a sparsing threshold $\gamma = 0.2$. On average, fewer than 25 coefficients were kept in the impulse response estimate. $M = 2N_t$ observations were needed to obtain good results in this experiment. An overall data rate of 30 kb/s (31.4 kb/s without pilot tones) is obtained for $K = 4096$ after coding, which proved to be essential in this experiment due to the high noise level. Almost no degradation in performance was observed without the use of pilot tones, except for $K = 4096$. Regarding the selection of M_t and M_f, we observe that the best results are obtained when only the frequency coherence is exploited $M = 1 \times M_f$, and for lower values of K. The other choices obviously result in a poorer performance.

In this experiment, it sufficed to use a single phase estimate for both transmitters. To illustrate this fact, Fig. 8 shows the

TABLE IV
EXPERIMENT 2: RESULTS FOR SEVERAL MIMO CONFIGURATIONS WITH TWO TRANSMITTERS (600 m). BER IS INDICATED FOR EACH $(M_t \times M_f)$ CONFIGURATION

$\mathbf{K}$	**1024**	**2048**	**4096**
$\mathbf{\Delta f}[Hz]$	61	30.5	15.3
$\mathbf{T}[ms]$	16.4	32.8	65.5
BER (1×4)	0	$7{\times}10^{-4}$	$6{\times}10^{-3}$
BER (2×2)	10^{-3}	$2{\times}10^{-3}$	$7{\times}10^{-3}$
BER (4×1)	$4{\times}10^{-3}$	$5{\times}10^{-3}$	$4{\times}10^{-2}$

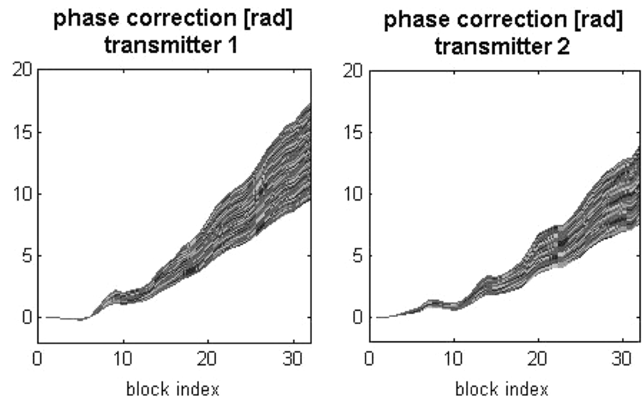

Fig. 8. Phase estimates in Experiment 2 for all carriers for a frame with $K = 1024$ at a transmission distance of 600 m.

phase estimates calculated independently for the two transmitters. The Doppler factors range between 0 and 4×10^{-5}, but the two sets of phase estimates are quite similar, leading to a similar performance with and without individual phase estimation for each transmitter.

C. Experiment 3: Narragansett Bay, RI

The data were recorded as part of the "RACE'08" experiment, conducted in the Narragansett Bay, RI, in March 2008. The transmitter and the receiver were fixed on the bottom, at a height of 3 and 2 m, respectively, in water depth ranging from 9 to 14 m. Signals were transmitted from two elements, separated by 60 cm, and collected at a distance of 400 and 1000 m using a vertical receiving array of six elements, equally spaced by 10 cm. The bandwidth was 10–12.5 kHz. The sampling rate was 39 062.5 Hz.

In this experiment, $N_d = 16\,384$ QPSK symbols per frame were transmitted from each transmitter, using 128 and 256 carriers. The guard interval was chosen to be $T_g = 15$ ms. The signals were coded using the BCH(64,10) code.

As indicated in Table V, error-free performance is obtained with both 128 and 256 carriers. The selection of M_f and M_t was not critical in this experiment, and no pilot tones were used. In Fig. 9, performance is detailed for one of the transmitters with $K = 256$ and $M_t \times M_f = 1 \times 4$. The uncoded BER is below 0.1, allowing the receiver to operate in decision-directed mode even without the decoder in the loop. Channel sparsing reduces the number of significant coefficient to four only, as this experiment is characterized by a relatively benign channel and narrow bandwidth. In this experiment, 8-PSK signals were also used, resulting in error-free performance with $K = 256$ and $M_t \times M_f = 1 \times 4$; however, coding is necessary to maintain decision-directed operation in this case.

D. Discussion

The results presented indicate that the optimal choice of system parameters varies with each experimental setting, and should be chosen accordingly. Nonetheless, the algorithm proposed is relatively simple, and general rules can easily be established for selecting its parameters M_t and M_f. Nonuniform phase estimation is essential for enabling the decision-directed operation, which, in turn, allows for a reduction in the pilot overhead. When implemented in a MIMO configuration, an independent phase estimate should be associated with each transmitter to take into account the possibility of different Doppler effect. As for the MIMO channel estimation, the number of observations needed to estimate the channel coefficients is at least $M = N_t$, while $M = 2N_t$ sufficed in all the experiments in our study. We found that fixed window can be used in frequency to reduce the computational complexity in the majority of the cases studied, while sliding window has to be used in time. Adaptive filtering (smoothing) further improves the channel estimates and is not overly sensitive to the choice of filter memory ($\lambda = 0.1$ was used in all cases). Sparsing of the impulse response provided performance improvement with the same truncation threshold in all cases ($\gamma = 0.2$). Finally, the general system design should target the largest number of carriers K for which temporal coherence can be maintained.

IV. CONCLUSION

MIMO communications were considered as a means of spatial multiplexing to increase the data rate supported by a bandlimited underwater acoustic channel. OFDM was used as a modulation technique that renders each subband free of intersymbol interference, thus simplifying the problem of MIMO channel estimation and enabling low-complexity coherent detection of PSK/quadrature amplitude modulation (QAM) signals.

The proposed algorithm incorporates compensation of the motion-induced nonuniform Doppler frequency offset across the wide acoustic signal bandwidth and adaptive MIMO channel estimation which capitalizes on the frequency correlation between adjacent carriers and time correlation between adjacent OFDM blocks. In this low-complexity approach, a single matrix inversion of size $N_t \times N_t$ (number of transmitters) is required per carrier, and these operations can be performed in parallel for the K carriers. The estimated frequency-domain (transfer function) coefficients are transformed into time-domain (impulse response) coefficients, where magnitude truncation is performed to account for the channel sparseness. Phase prediction enables decision-directed operation, resulting in a significant reduction in the pilot overhead.

Receiver operation was demonstrated using experimental data from three collection sites, all corresponding to shallow-water channels with a range on the order of 1 km, but with different frequency bands. The data were analyzed to

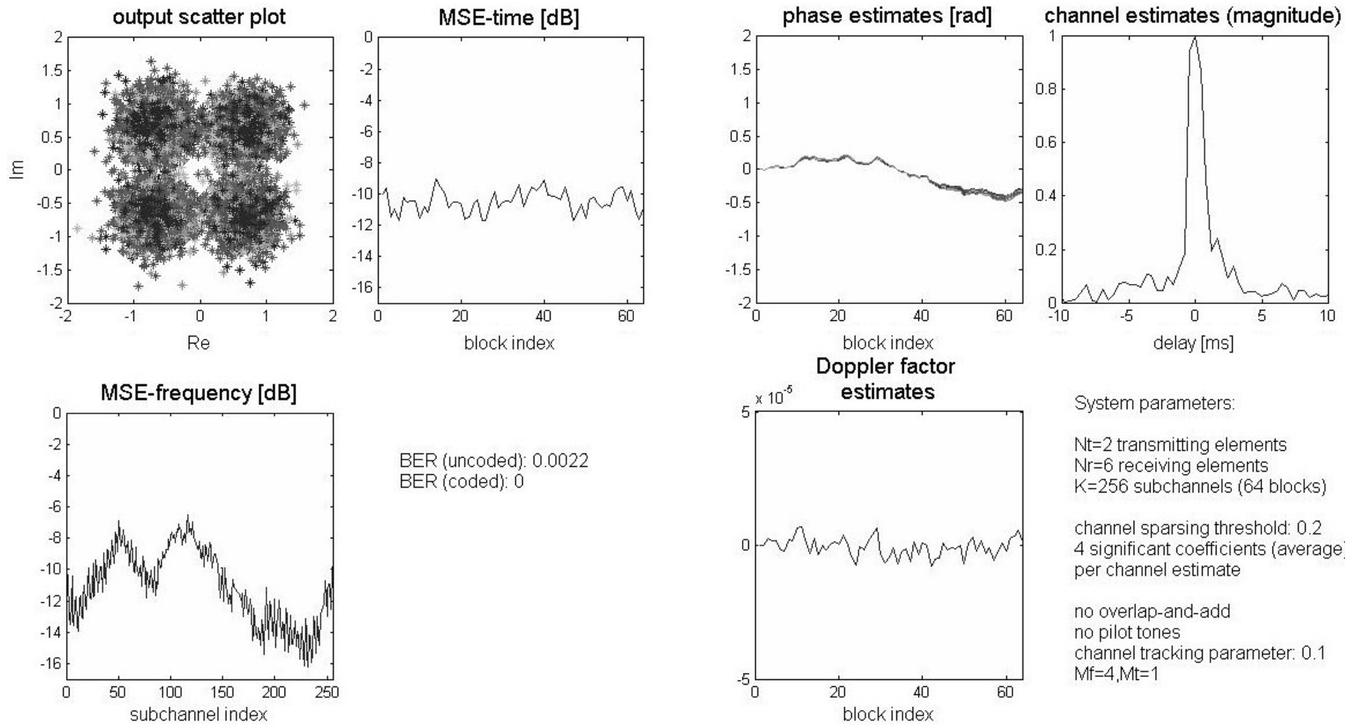

Fig. 9. Signal processing results for Experiment 3 at a transmission distance of 1 km.

TABLE V
EXPERIMENT 3: RESULTS FOR SEVERAL MIMO CONFIGURATIONS WITH TWO TRANSMITTERS (1000 m). BER IS INDICATED FOR EACH $(M_t \times M_f)$ CONFIGURATION

$\mathbf{K}$	**128**	**256**
$\mathbf{\Delta f}[Hz]$	19.1	9.5
$\mathbf{T}[ms]$	52.4	104.9
BER (1×4)	0	0
BER (2×2)	0	0
BER (4×1)	0	0

assess the system performance with a varying number of carriers K, and a varying number of adjacent frequency bands M_f and adjacent time blocks M_t needed for channel estimation. To maximize the bandwidth efficiency, the number of carriers should be chosen as the greatest K for which the channel coherence can still be exploited [i.e., condition (27) is satisfied]. Specifically, for the experimental signals at hand, this design yielded a QPSK bandwidth efficiency of about 1.5 b/s/Hz per transmit element, and led in general to the $M_t = 1$ solution. With the BCH(64,10) code, nearly error-free performance was observed consistently in all experiments. The attendant bit rates after coding were 18.9 kb/s (four transmitters and 1024 carriers in 24-kHz bandwidth), 26.8 kb/s (two transmitters and 2048 carriers in 62.4-kHz bandwidth), and 2.1 kb/s (two transmitters and 256 carriers in 2.4-kHz bandwidth, 8PSK).

Future work on MIMO–OFDM signal processing for underwater acoustic channels will focus on designing alternative channel estimation methods, and assessing the spatial correlation properties to identify fundamental limitations in capacity increase through MIMO signal processing.

APPENDIX

A. Algorithm Summary

The following steps summarize the algorithm operation. These steps should be carried out at every iteration $n = M_t, M_t+1, \ldots$, corresponding to the detection of the nth OFDM block. The algorithm is initialized using known data symbols during $n = 0, \ldots, M_t - 1$. The phase estimates $\hat{\theta}_k^t$ and the Doppler factors $\hat{a}^t$ are set to 0 during initialization.

1) Using the existing channel estimates, form

$$\mathbf{c}_k(n) = [\tilde{\mathbf{H}}_k'(n-1)\tilde{\mathbf{H}}_k(n-1)]^{-1}\tilde{\mathbf{H}}_k'(n-1)\mathbf{y}_k(n). \quad (36)$$

The channel estimate $\tilde{\mathbf{H}}_k$ is an analog of (6) obtained from the truncated (sparse) impulse response via (35).

2) Make tentative symbol decisions using a prediction of the phase offset and the existing channel estimates

$$\check{\theta}_k^t(n) = \hat{\theta}_k^t(n-1) + \hat{a}^t(n-1)2\pi f_k T' \qquad \forall k,t \quad (37)$$
$$\overline{d}_k^t(n) = \mathrm{dec}[c_k^t(n)e^{-j\check{\theta}_k^t(n)}] \qquad \forall k,t. \quad (38)$$

The function $\mathrm{dec}[\cdot]$ indicates soft-decision decoding in general. If pilots are available, use them instead of tentative decisions.

3) Update the phase estimates.
   - Measure the phase error as the angle (argument)

$$\psi_k^t(n) = \left\langle c_k^t(n)e^{-j\hat{\theta}_k^t(n-1)}\overline{d}_k^{t*}(n)\right\rangle \qquad \forall k,t. \quad (39)$$

   The phase error can further be filtered as in [1].
   - Estimate the Doppler factor

$$\hat{a}^t(n) = \frac{1}{K}\sum_k \frac{\psi_k^t(n)}{2\pi f_k T'} \qquad \forall t. \quad (40)$$

Note that fewer than K terms can be used to perform the above averaging, depending on the number of reliable data symbols available at this time.

- Update the phases

$$\hat{\theta}_k^t(n) = \hat{\theta}_k^t(n-1) + \hat{a}^t(n)2\pi f_k T' \qquad \forall k, t. \quad (41)$$

4) Make symbol decisions (refined)

$$\tilde{d}_k^t(n) = \text{dec}\left[c_k^t(n)e^{-j\hat{\theta}_k^t(n)}\right] \qquad \forall k, t. \quad (42)$$

5) Update the channel estimates.
   - For all carriers, form the matrix $\check{\mathbf{D}}_k(n)$ using the phase and data estimates instead of true values in (24); form the vector $\check{\mathbf{y}}_k(n)$ of the received signals, and calculate the instantaneous channel estimate (17) if fixed window is used or (18) if sliding window is used.
   - Compute the channel impulse response and update the channel (31) using inverse FFT (IFFT) (33).
   - Identify the significant terms of impulse response estimates and set the rest to zero (34).
   - Calculate the transfer function coefficients $\tilde{\mathbf{H}}_k(n)$ (35).

ACKNOWLEDGMENT

The authors would like to thank the Woods Hole Oceanographic Institution's acoustic communications group for conducting at-sea experiments. They would also like to thank anonymous reviewers for providing constructive remarks.

REFERENCES

[1] M. Stojanovic, "Low complexity OFDM detector for underwater acoustic channels," in *Proc. IEEE OCEANS Conf.*, Sep. 2006, DOI: 10.1109/OCEANS.2006.307057.

[2] B. Li, S. Zhou, M. Stojanovic, L. Freitag, and P. Willett, "Multicarrier communication over underwater acoustic channels with nonuniform Doppler shifts," *IEEE J. Ocean. Eng.*, vol. 33, no. 2, pp. 198–209, Apr. 2008.

[3] M. Stojanovic, "OFDM for underwater acoustic communications: Adaptive synchronization and sparse channel estimation," in *Proc. Int. Conf. Acoust. Speech Signal Process.*, 2008, pp. 5288–5291.

[4] B. Li, S. Zhou, M. Stojanovic, L. Freitag, J. Huand, and P. Willett, "MIMO-OFDM over an underwater acoustic channel," in *Proc. IEEE OCEANS Conf.*, Oct. 2007, DOI: 10.1109/OCEANS.2007.4449296.

[5] M. Stojanovic, "MIMO OFDM over underwater acoustic channels," in *Proc. 43rd Asilomar Conf. Signals Syst. Comput.*, Nov. 2009, pp. 605–609.

[6] R. Ormondroyd, "A robust underwater acoustic communication system using OFDM-MIMO," in *Proc. IEEE OCEANS Conf.*, Jun. 2007, DOI: 10.1109/OCEANSE.2007.4302422.

[7] Y. Li, N. Seshadri, and S. Ariyavisitakul, "Channel estimation for OFDM systems with transmitter diversity in mobile wireless channels," *IEEE J. Sel. Areas Commun.*, vol. 17, no. 3, pp. 461–471, Mar. 1999.

[8] H. Minn, D. Kim, and V. K. Bhargava, "A reduced complexity channel estimation for OFDM systems with transmit diversity in mobile wireless channels," *IEEE Trans. Commun.*, vol. 50, no. 5, pp. 799–807, May 2002.

[9] Y. G. Li, "Simplified channel estimation for OFDM systems with multiple transmit antennas," *IEEE Trans. Wireless Commun.*, vol. 1, no. 1, pp. 67–75, Jan. 2002.

[10] M. Tsatsanis and G. Giannakis, "Modeling and equalization of rapidly fading channels," *Int. J. Adapt. Control Signal Process.*, vol. 10, pp. 159–176, Mar. 1996.

[11] D. Borah and B. Hart, "Frequency-selective fading channel estimation with a polynomial time-varying channel model," *IEEE Trans. Commun.*, vol. 47, no. 6, pp. 862–873, Jun. 1999.

[12] T. Zemen and C. Mecklenbrauker, "Time-variant channel estimation using discrete prolate spheroidal sequences," *IEEE Trans. Signal Process.*, vol. 53, no. 9, pp. 3597–3607, Sep. 2005.

[13] I. Barhumi, G. Leus, and M. Moonen, "Optimal training design for MIMO OFDM systems in mobile wireless channels," *IEEE Trans. Signal Process.*, vol. 51, no. 6, pp. 1615–1624, Jun. 2003.

[14] S. Cotter and B. Rao, "Sparse channel estimation via matching pursuit with application to equalization," *IEEE Trans. Commun.*, vol. 50, no. 3, pp. 374–377, Mar. 2002.

[15] A.-B. Salberg and A. Swami, "Doppler and frequency-offset synchronization in wideband OFDM," *IEEE Trans. Wireless Commun.*, vol. 4, no. 6, pp. 2870–2881, Nov. 2005.

[16] B.-C. Kim and I.-T. Lu, "Parameter study of OFDM underwater communications system," in *Proc. IEEE OCEANS Conf.*, Sep. 2000, vol. 2, pp. 1251–1255.

[17] M. Stojanovic, "Underwater acoustic communications: Design considerations on the physical layer," in *Proc. 5th Annu. Conf. Wireless Demand Netw. Syst. Services*, Jan. 2008, DOI: 10.1109/WONS.2008.4459349.

Patricia Ceballos Carrascosa was born in Logroño, Spain, in 1984. She received the Engineering Degree in telecommunication engineering and the M.S. degree in information and communication technologies from the Polytechnical University of Catalonia (UPC), Catalonia, Spain, in 2008.

From September 2007 to May 2008, she was a Visiting Researcher at the Massachusetts Institute of Technology (MIT), Cambridge, under the supervision of Prof. M. Stojanovic on signal processing for underwater communications. Her research interests include antennas, electromagnetic scattering and imaging, wireless systems, and signal processing. She is currently working in strategic consulting.

Milica Stojanovic (S'90–M'93–SM'08–F'10) graduated from the University of Belgrade, Belgrade, Serbia, in 1988, and received the M.S. and Ph.D. degrees in electrical engineering from Northeastern University, Boston, MA, in 1991 and 1993.

After a number of years with the Massachusetts Institute of Technology (MIT), Cambridge, where she was a Principal Scientist, she joined the faculty of the Electrical and Computer Engineering Department, Northeastern University, in 2008. She is also a Guest Investigator at the Woods Hole Oceanographic Institution (WHOI), Woods Hole, MA, and a Visiting Scientist at MIT. Her research interests include digital communications theory, statistical signal processing and wireless networks, and their applications to underwater acoustic communication systems.

Dr. Stojanovic is an Associate Editor for the IEEE JOURNAL OF OCEANIC ENGINEERING and the IEEE TRANSACTIONS ON SIGNAL PROCESSING.